Nuclear Instruments and Methods in Physics Research A 371 (1996) 449–459

NUCLEAR INSTRUMENTS & METHODS IN PHYSICS RESEARCH Section A

ELSEVIER

High resolution gamma-ray spectroscopy with a radioactive beam

W.N. Catford[a,*], S. Mohammadi[a,1], P.H. Regan[a], C.S. Purry[a], W. Gelletly[a], P.M. Walker[a], G.J. Gyapong[a], J. Simpson[b], D.D. Warner[b], T. Davinson[c], R. Neal[c], R.D. Page[c,2], A.C. Shotter[c], I.M. Hibbert[d], R. Wadsworth[d], S.A. Forbes[e,3], A.M. Bruce[f], C. Thwaites[f], P. Thirolf[g], P. Van Duppen[h], W. Galster[i], A. Ninane[i], J. Vervier[i], P. Decrock[j], M. Huyse[j], J. Szerypo[j,4], J. Wauters[j]

[a]*Department of Physics, University of Surrey, Guildford, Surrey, GU2 5XH, UK*
[b]*CCLRC, Daresbury Laboratory, Daresbury, Warrington, WA4 4AD, UK*
[c]*Department of Physics, University of Edinburgh, Edinburgh, EH9 3JZ, UK*
[d]*Department of Physics, University of York, York, YO1 5DD, UK*
[e]*Oliver Lodge Laboratory, Department of Physics, University of Liverpool, Liverpool, L69 3BX, UK*
[f]*Department of Mathematical Sciences, University of Brighton, Brighton, BN2 4GJ, UK*
[g]*Max Planck Institute für Kernphysik, D-6900 Heidelberg, Germany*
[h]*ISOLDE-CERN, PPE Division, CH-1211 Geneva 23, Switzerland*
[i]*Institut de Physique Nucléaire and Centre de Recherches du Cyclotron, Université Catholique de Louvain, B-1348 Louvain-la-Neuve, Belgium*
[j]*Instituut voor Kern- en Stralingsfysica, Katholieke Universiteit Leuven, B-3001 Leuven, Belgium*

Received 7 September 1995

Abstract

The γ-rays de-exciting the yrast states in neutron deficient nuclei around $A \sim 55$ have been observed from fusion-evaporation reactions induced by an intense radioactive ^{19}Ne beam on a ^{40}Ca target. An array of escape suppressed germanium detectors recorded reaction γ-rays. Background subtraction of radiation from the decay of the beam was achieved using the timing properties of the pulsed beam and through particle detection using the LEDA charged particle array. These data constitute the first use of an on-line separated and accelerated radioactive beam for studies of near yrast nuclear states using fusion-evaporation reactions. Information on the γ-ray yields from evaporation residues, relative to yields with a stable beam, has been obtained and the problems associated with performing such experiments in a highly radioactive background environment have been addressed.

1. Introduction

Heavy ion fusion-evaporation reactions have proved to be an invaluable tool in the study of high-spin yrast and near-yrast nuclear states [1,2]. Until now, the final nuclei populated in such experiments have been limited essentially by the availability of only stable beam and target ion species. For example, one of the current problems with investigating $N \sim Z$ nuclei is that the restriction to stable beams and targets forces the use of reactions with very low cross sections. These usually involve the evaporation of two or more neutrons from the compound nucleus in order to reach the most neutron deficient nuclei. Larger cross sections are expected for the population of $N = Z$ nuclei if neutron deficient radioactive beams are used since in this case fewer neutrons have to be emitted to reach the same final nucleus. Much effort is presently being devoted to the design and construction of radioactive beam facilities in Europe [3–5], North America [6–10] and Japan [11,12], following pioneering work at laboratories such as Louvain-la-Neuve [13,14]. By colliding neutron deficient beams with suitable stable target nuclei, it should be possible to investigate the detailed structure of nuclei close to the proton drip line which are presently inaccessible. Similarly, the neutron rich side of stability simply cannot be

* Corresponding author. Tel +44 1483 259323, fax +44 1483 259601, e-mail w.catford@ph.surrey.ac.uk.

[1] On leave from: Department of Physics, Payam-Noor University, Fariman 93914-33, Iran.

[2] Present address: Oliver Lodge Laboratory, Department of Physics, University of Liverpool, L69 3BX, UK.

[3] Present address: Consultancy Services, AEA Technology, Harwell, Didcot, Oxon. OX11 0RA, UK.

[4] Present address: Institute of Experimental Physics, Warsaw University, Hoza 69, PL-00-681 Warsaw, Poland.

SSDI 0168-9002(95)00857-8

reached using stable projectiles, and neutron rich radioactive beams offer exciting possibilities.

In order to assess the utility of radioactive beams at energies close to the Coulomb barrier a number of questions must be addressed experimentally. For studies using neutron-deficient beams, these include: (a) the effect of a more neutron deficient compound system on the relative yield of evaporation products; (b) the high background produced from the decay of the scattered beam; (c) the (initially) lower values of beam intensity; and (d) the effect of using charged particle detection devices and beam pulsing to improve signal to noise ratios and channel selection. Gamma-ray studies using neutron-rich beams will in some ways be simpler since any scattered beam will produce a β-decay background with no flux of 511 keV γ-rays. In the present work we report on the first use of an on-line-separated, accelerated radioactive ion beam in high resolution γ-ray spectroscopy. A fusion-evaporation reaction has been employed in conjunction with an array of germanium detectors to study neutron deficient nuclei around $N \sim Z \sim 28$. The general conclusions should prove useful in planning future studies of γ-ray spectroscopy using radioactive beams.

2. Experimental setup

A schematic diagram of the experimental set-up is shown in Fig. 1. Gamma-rays were recorded from residual nuclei formed in reactions on a ^{40}Ca target using a ^{19}Ne beam produced at the Louvain-La-Neuve radioactive ion beam facility. The ^{19}Ne projectiles decay via β^+ emission to ^{19}F with a half-life of 17 s. A preliminary experiment was performed using a ^{19}F beam incident on the same target, in order to compare the ^{19}Ne results with those from a stable beam.

The ^{19}Ne beam was produced at Louvain-la-Neuve in a two stage process [13,14]. Briefly, the CYCLONE 30 cyclotron produced 30 MeV protons with a beam current of 150 μA. This primary beam bombarded a thick lithium fluoride target to produce the species of interest via the ^{19}F(p, n)^{19}Ne reaction. The target was kept molten by the beam heating (melting point 1118 K) and was enclosed in a graphite cylinder which became transparent to neon atoms at high temperature. Reaction products that diffused from the target were pumped to an electron cyclotron resonance (ECR) ion source. Ions with $A = 19$ in the 4+ charge state were magnetically selected and injected into CYCLONE. This variable energy cyclotron ($K = 110$) was operated in third harmonic mode to provide the required bombarding energy of 70 MeV. Initially, CYCLONE was tuned to accelerate a beam of ~10 p nA of $^{19}F^{4+}$ ions for optimisation of the operating conditions, and afterwards the magnetic field was adjusted to accelerate ^{19}Ne. Using this method, beams of up to 150 p pA (9.4×10^8 particles per second) of $^{19}Ne^{4+}$ were accelerated to an energy of 70 MeV. The final focus at the target position was 5 mm in diameter and the beam was pulsed to provide 2 ns wide (fwhm) beam bursts separated by 73 ns. This radioactive beam was incident on a 1.6 mg/cm^2 self-supporting ^{40}Ca metal target which was stored in vacuum prior to use. The energy of the beam was above the Coulomb barrier for this system (at $E_{beam} \simeq 58$ MeV), thus allowing fusion-evaporation reactions.

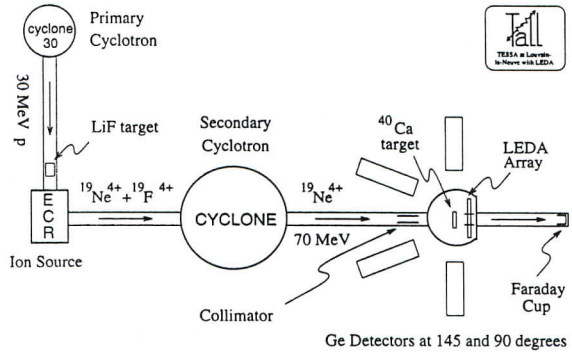

Fig. 1. Schematic diagram of the experimental layout. The secondary cyclotron could be tuned to provide either a $^{19}Ne^{4+}$ beam (as shown) or a $^{19}F^{4+}$ beam.

Gamma-rays emitted from transitions in the residual nuclei were detected by an array of 7 escape suppressed germanium (Ge) detectors of the TESSA geometry [15]. The Ge detectors had efficiencies between 20% and 25% (for 1332 keV radiation, relative to a 76 mm × 76 mm NaI detector at 250 mm). The detectors were mounted at angles of 90° and 145° with respect to the beam direction with their front faces 230 mm from the target. Preliminary tests with ^{19}Ne had confirmed that the 511 keV annihilation radiation from the scattered beam was sufficient to saturate the bismuth germanate (BGO) suppression shields of the Ge array. This was largely the result of the particular properties of the CYCLONE beam, which necessitated a final collimator near the target in addition to that located further upstream. This arrangement led to a small percentage of the beam being stopped near the entrance of the target chamber. It is estimated that 5% of the primary beam particles were stopped on the final beam collimators, 150 mm before the target. This amounted to 4.7×10^7 pps, and hence 47 MBq of ^{19}Ne activity (94 million 511 keV γ-rays per second) within the ring of 145° detectors in the Ge array. Thus, a 20 mm thickness of Pb shielding was fitted around each of the BGO suppression shields and around the beam collimators. An inner layer of 1 mm of Sn surrounded the BGO shields in order to attenuate Pb X-rays. The beam stop was 2 m behind the target position and well shielded from the γ-ray detectors with a wall of lead bricks.

In order to provide some channel selection according to

atomic number, Z, of the residual nuclei produced, coincidences between gamma-rays and evaporated light charged particles were measured. Charged particles were detected by an array of 128 silicon strip segments arranged in an octagonal shape (the LEDA array [16,17]) and placed in the forward direction. The 128 annular segments spanned the range of angles from 19° to 42° relative to the beam direction and were 300 μm thick. The perpendicular distance from the target was 150 mm. The high granularity of this device allowed information on multiple charged particle events to be obtained. In this configuration, the geometric efficiency of the LEDA array for detecting individual protons and alpha-particles was approximately 10%. Aluminium stopping foils of thickness 11.7 mg/cm^2 were used to shield the strip detectors from scattered beam. Some data were also collected without stopping foils and exhibited a prohibitively high rate of random coincidences with the γ-ray detectors. All of the components except the Ge detectors and their shields were housed in vacuum.

The arrangement of the LEDA array in the forward hemisphere and the γ-ray detectors in the backward hemisphere was convenient experimentally. In addition, it was partly designed to combat the background due to beam particles scattering at angles $\gtrsim 15°$ in the target and stopping in the target chamber or on the inside of the beam line near the chamber. By calculating the integrated Rutherford scattering cross section backward of 15°, with the beam intensity and target thickness employed in the experiment, the 511 keV γ-ray activity from this source was estimated to be a factor of approximately 1000 less than the activity resulting from the beam deposited on the collimators. Taking into account the effect of the Pb shielding, the background from the collimators still dominated by at least an order of magnitude. In future work, with better focussing, the management of the elastically scattered beam may be a vital part of the experimental design.

Initial calibrations of the apparatus and the method of analysis were performed using radioactive sources and sharp γ-ray peaks from the $^{19}F + ^{40}Ca$ reaction. The electronics was configured to accept only Compton suppressed Ge events. Event triggers were constructed for γ-singles, γ–γ, and γ–LEDA coincidences. In practice, the low event rate meant that the data acquisition system was able to collect all Compton suppressed γ-ray singles events. Event-by-event data were recorded on EXABYTE tapes for subsequent off-line analysis. The parameters recorded were the energies of any Ge detector or LEDA strip that fired, and the relative times of each. For LEDA the timing signal was generated by the first strip to fire, and in all cases the RF of the cyclotron provided the timing reference. Table 1 shows the typical rates for the various parameters with each of the beams employed. The exposure time to the ^{19}F beam was 12 hours, and this was followed by 43 hours of exposure to the radioactive ^{19}Ne beam.

Table 1
Typical counting rates with beam on target

Beam	Current [p nA]	Σ (Ge)[a] [kHz]	Σ (LEDA)[b] [kHz]	LEDA–Ge[c] [Hz]	Ge–Ge[d] [Hz]
^{19}F	12.50	25	250	6500	250
^{19}Ne	0.12	4	5	70	10

[a] Sum of seven Ge detectors after Compton suppression.
[b] Sum of 128 strips.
[c] Coincidence of any suppressed Ge with any LEDA strip.
[d] Any coincidence of at least two suppressed Ge detectors.

3. Data analysis and results

3.1. Compton suppressed γ-ray energy spectra

The Compton suppressed γ-ray energy spectrum, as acquired directly from the TESSA Ge detectors, is shown in Fig. 2a. This spectrum represents the combined data from all 90° detectors after gain matching, acquired with the ^{19}Ne beam. As anticipated the spectrum is dominated by 511 keV annihilation radiation which eluded both the extensive Pb shielding and also the BGO shields, and entered the Ge detectors. It can be seen, however, that the

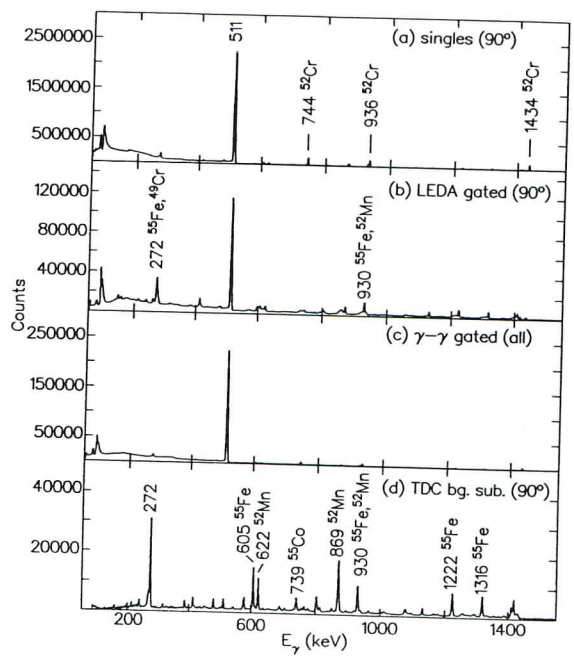

Fig. 2. Gamma ray energy spectra from the $^{19}Na + ^{40}Ca$ reaction: (a) all singles, (b) in coincidence with charged particles, (c) in coincidence with other γ-rays, and (d) singles with full background subtraction as described in the text. The spectra comprise combined data from all 90° Ge detectors, except (c) which also includes 145° detectors.

annihilation quanta interacting in the BGO shield did not preclude effective Compton suppression, since the Compton edge for 511 keV γ-rays at 341 keV is not observed to any substantial degree. (The rates in individual BGO shields were >60 kHz.) The source of the 511 keV background, it should be remembered, was the small fraction of beam that scattered and stopped near the array and that β^+-decayed. In particular, the final beam collimation into the target chamber and also stray beam particles hitting inside the beam line were major contributors, and hence these γ-rays were often entering the Ge detectors through the BGO suppression shields and not through the front face.

Apart from the dominant 511 keV counts and low energy X-rays from Pb and Bi, the singles spectrum in Fig. 2a also shows peaks due to radioactivity in the target. The peaks identified as ^{52}Cr transitions arise from the β^+-decay of ^{52}Mn fusion-evaporation products ($T_{1/2} = 42$ min). In the present experiment, this contribution was exacerbated by the same target being employed both for the setting up with the stable ^{19}F beam, and for the ^{19}Ne running.

Finally, in the ungated spectrum of Fig. 2a, the peaks due to the strongest reaction γ-rays are just discernible. These are found to arise from the fusion-evaporation nuclei predicted to have the largest cross sections according to the statistical code PACE [18], namely ^{55}Co (3pn evaporation, [19]), ^{55}Fe (4p, [20]), ^{54}Fe (4pn, [21]), and ^{52}Mn (α3p, [22]). The largest reaction peak is at 272 keV (^{55}Fe [20], ^{49}Cr [23]).

3.2. Simple coincidence gating

It is instructive to see the effect on the γ-ray spectra of particle–γ or γ–γ coincidence requirements. These could offer a simple means of highlighting reaction γ-rays and could prove particularly useful during on-line data acquisition. A particle–γ coincidence indicates the occurrence of a fusion-evaporation reaction. Any radioactivity γ-rays emitted between beam pulses, or indeed emitted during beam pulses in which no reaction was induced, are discriminated against – but at a cost due to the <100% efficiency of detecting at least one charged particle (~10–35% in this experiment, depending on the charged particle multiplicity). The effectiveness of a γ–γ coincidence requirement in discriminating against annihilation quanta depends on the detector geometry around the sites of the β^+ activity. In the case of beta-delayed γ-rays from radioactivity build up in the target any effectiveness is achieved only in so far as the average γ-ray multiplicity following β^+-decay is likely to be less than for reaction events.

The effect of particle–γ gating is shown in Fig. 2b and the effect of the γ–γ requirement (where at least two Ge detectors fire) is shown in Fig. 2c. The particle–γ requirement is seen to be a good first-order tool for selecting reaction γ-rays. The coincidence requirement was implemented in the computer software by checking each of the LEDA channels to see if its analog-to-digital converter had encoded. Fast-coincidence logic was not employed due to the large variation (~0.1 μs) in particle flight times to the LEDA detectors, according to their energy and mass. Figs. 3a and 3b show in more detail the substantial removal of activity lines from the γ-ray energy spectrum by particle gating. An activity spectrum, acquired over a period of 25 minutes with no beam on target, is also shown for comparison. The effectiveness of the particle gating is related to the dominance of charged particle emission during evaporation from the compound nucleus and to the low beam intensity. Whilst essentially every fusion-evaporation event produced charged particles in the present experiment, each beam pulse contained fewer than 100 incident nuclei and thus most pulses initiated no reaction of interest. A further feature of the reaction peaks in Fig. 3 is the presence of Doppler-broadened lineshapes indicating nuclear lifetimes of the order of several hundred femtoseconds for the decaying states. For example, in Fig. 3d the peak at 801 keV has a shoulder extending down by approximately 20 keV ($=\beta\cos(145°)\times E_\gamma$) below the unshifted energy. These lineshapes are evident in Fig. 3 because the data from all the Ge detectors (including those

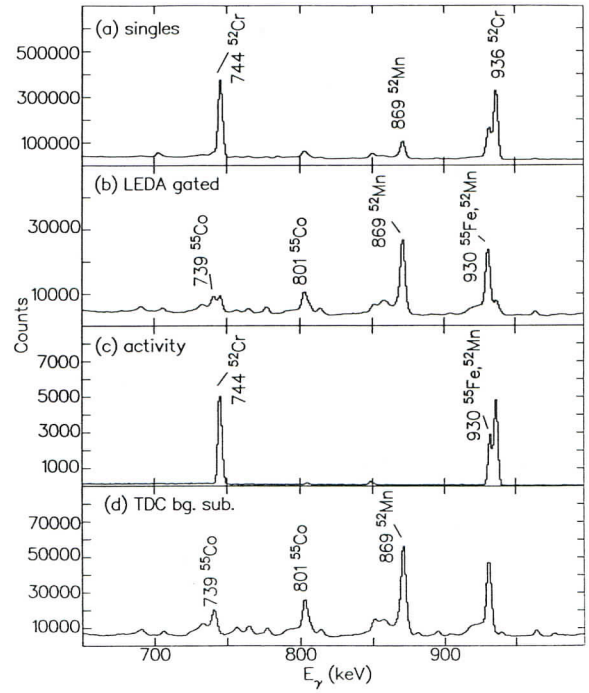

Fig. 3. Detail of background subtraction for the gamma ray energy spectrum from the ^{19}Ne + ^{40}Ca rection: (a) all singles, (b) in coincidence with charged particles, (c) for comparison, a spectrum of radioactivity with the beam off, and (d) singles with full background subtraction as described in the text. The spectra comprise combined data from all Ge detectors.

at 145°) have been combined. Most recoiling nuclei were either stopped or else slowed down significantly in the target prior to γ-decaying. This distortion due to lifetime effects must be anticipated whenever an attempt is made to compensate for the low intensity of a radioactive ion beam by employing a thick target.

3.3. Fully background-subtracted γ-ray singles spectra

The most effective elimination of non-reaction counts from the γ-ray energy spectra was achieved using the measurements of γ-ray timing relative to the beam pulses. Both the need for this, and the reason for its high effectiveness, are well illustrated in the timing spectra of Fig. 4. The upper part of the figure shows that reaction γ-rays (which give counts only in the peaks corresponding to the beam pulses) are detected amidst a large continuous flux of radioactivity γ-rays. The peaks for the beam pulses are 8 ns wide FWHM (limited by the timing performance of the Ge detectors) and separated by 73 ns. In Fig. 4b the continuous underlying flux of coincidence γ–γ events due to radioactivity is shown.

Fig. 4c illustrates the vast difference between stable and radioactive beam experiments. With the stable beam, the number of particles per pulse was two orders of magnitude higher and the beam itself was not a source of annihilation quanta.

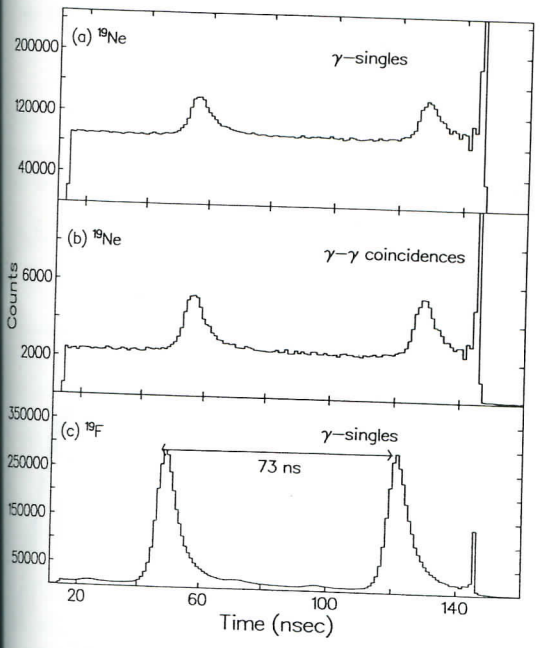

Fig. 4. Timing spectra for γ-rays relative to the beam pulse. The electronics distributed the true in-beam events evenly between the two peaks for odd and even numbered beam pulses. The spike above channel 140 is also an artefact of the electronics. Spectra are shown for (a) single γ-rays and (b) γ–γ coincidence events for the ^{19}Ne beam, and (c) singles γ-rays for the ^{19}F beam.

The γ-ray energy spectrum in Fig. 2d spectacularly shows the effectiveness of software gating in which the continuous radioactive background has been removed. This was achieved by subtracting a spectrum recorded during the period between beam pulses from one recorded during the in-beam peak of the timing spectrum. The result is a spectrum of just the prompt γ-rays which are produced in the fusion-evaporation reactions. Gamma-ray energies down to 100 keV are accessible to study. After the background subtraction, the data set contained a total of 1.4×10^8 γ-ray singles events from the two day ^{19}Ne experiment.

3.4. Particle–γ channel selection

3.4.1. Overview

The pixellated nature of the LEDA array allowed multiple charged particle detection from the fusion-evaporation reactions. In addition, the evaporated protons and α-particles could be distinguished from each other on the basis of the energy they deposited in the silicon detectors. For protons, this was a maximum of 6 MeV, and for α-particles a maximum of 24 MeV, determined by the thickness of the detector. The energies predicted (using PACE [18]) for protons and α-particles extended to ~30 MeV but the evaporation of α-particles with energies below approximately 5 MeV was strongly suppressed due to tunnelling penetrability factors.

Particle–γ gating according to the charged particle multiplicity in LEDA, and according to particle type, has been performed. In the first instance, the number of charged particles evaporated with each γ-ray event could be clearly established. In the second case, significant further channel identification was possible since α-particles were distinguished from protons.

3.4.2. Charged particle multiplicity measurements

Individual γ-ray singles spectra of the type shown in Fig. 2d were produced for specific values of the number of charged particles observed in LEDA. The relative areas of γ-ray peaks in these spectra were then analysed for comparison with binomial probability distributions. The best overall fit to the data was obtained using a probability of 0.100 for each charged particle to hit the detector, which is consistent with near isotropic particle emission. The results are displayed in Table 2, and demonstrate that the charged particle multiplicity can be deduced for individual γ-ray peaks.

When the fit was restricted to the channels with proton emission, but no α-particle emission, the best fit probability was reduced to 0.088 ± 0.002 and the fits to the data were all easily consistent with the binomial distribution in a χ^2 test. Furthermore, the data served to identify the correct number of charged particles uniquely, allowing

Table 2
Comparison of LEDA hit probabilities with binomial calculations. Results are given for various specific gamma-ray transitions, identifying different nuclei with different numbers N_C of charged particles evaporated.

N_C	Channel	Nucleus	E_γ [keV]	Probability of n hits			
				$n=0$	$n=1$	$n=2$	$n=3$
3	B[a]			0.729	0.243	0.027	0.001
	3pn	^{55}Co	2973	0.761±0.021	0.216±0.020	0.022±0.002	0.001±0.001
	3p	^{56}Co	576	0.773±0.014	0.204±0.014	0.022±0.001	0.001±0.001
4	B[a]			0.656	0.292	0.049	0.004
	3pα	^{52}Mn	869	0.639±0.004	0.304±0.004	0.052±0.001	0.005±0001
	4p	^{55}Fe	1316	0.697±0.020	0.262±0.018	0.038±0.002	0.003±0.001
5	B[a]			0.590	0.328	0.073	0.008
	5p	^{54}Mn	156	0.610±0.031	0.316±0.029	0.066±0.016	0.007±0.002

[a] B means binomial probability calculated with a 10% hit probability.

alternative hypotheses to be rejected. The data for γ-ray peaks with associated α-particle emission implied that the probability for an α-particle to hit the detector was significantly higher than for a proton, indicating extra kinematic forward focussing for the α-particles consistent with their lower centre-of-mass velocities.

The charged particle multiplicity measurements thus go a long way towards allowing the evaporation channel to be assigned for each γ-ray peak.

3.4.3. Charged particle identification

As shown in Fig. 5, and discussed above, the energy deposited by α-particles was greater than that deposited by protons. The separation between protons and α-particles was further improved in the two-dimensional plots of pairs of LEDA energies produced for multiple charged particle events. Software gating allowed γ-ray energy spectra to be generated for specific charged particle criteria and examples are shown in Fig. 6. These spectra include full background subtraction as discussed in Section 3.3.

The charged particle coincidences are seen to be dominated by events with at least four charged particles emitted, including at least one proton. In particular, several lines from 4p evaporation to ^{55}Fe [20] are clearly visible in the proton-gated spectrum (Fig. 6a). In the α-particle gated spectrum (Fig. 6d) however, these lines are absent, whilst lines from the 3pα channel to ^{52}Mn [22] and the 2p2α channel to ^{49}Cr [23] are highlighted.

3.5. Full coincidence gating for γ–γ events

A total of 8.3×10^6 γ–γ coincidence events were obtained for the ^{19}Ne experiment. After software analysis including suitable background subtraction, a total of 7×10^4 γ–γ coincidences remained.

The background subtraction procedure was designed to subtract the contribution from coincidences in which at least one non-reaction γ-ray was included, i.e. a random 511 keV γ-ray or a β-delayed γ-ray. This background otherwise dominated the matrix. Background subtraction was performed off-line by gating on the various regions of the individual timing spectra for each detector as shown in

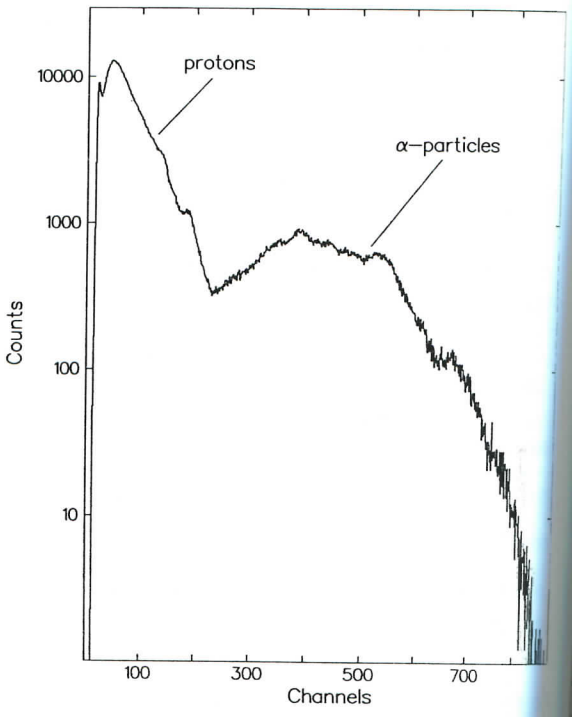

Fig. 5. Energy spectrum from one element of the LEDA array showing good separation between the energy deposited by protons and α particles.

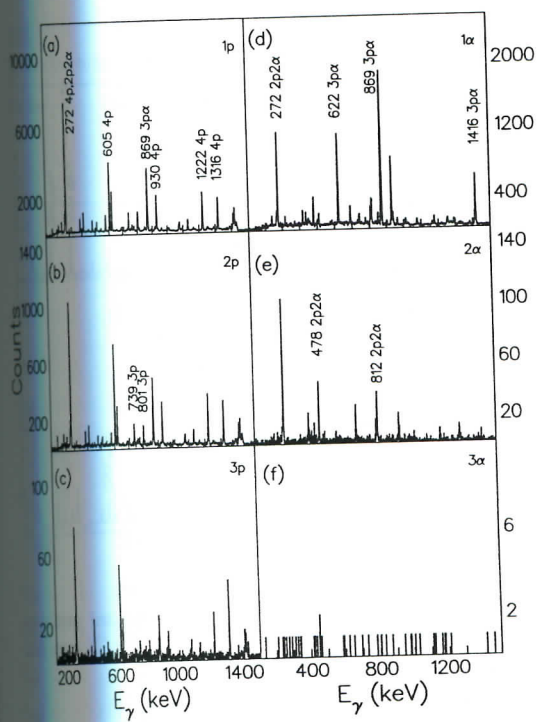

Fig. 6. Gamma-ray energy spectra with full background subtraction and with specific particle gating requirements: in coincidence with precisely (a) one, (b) two, and (c) three protons; in coincidence with precisely (d) one, (e) two, and (f) three α-particles. Data from all 90° Ge detectors.

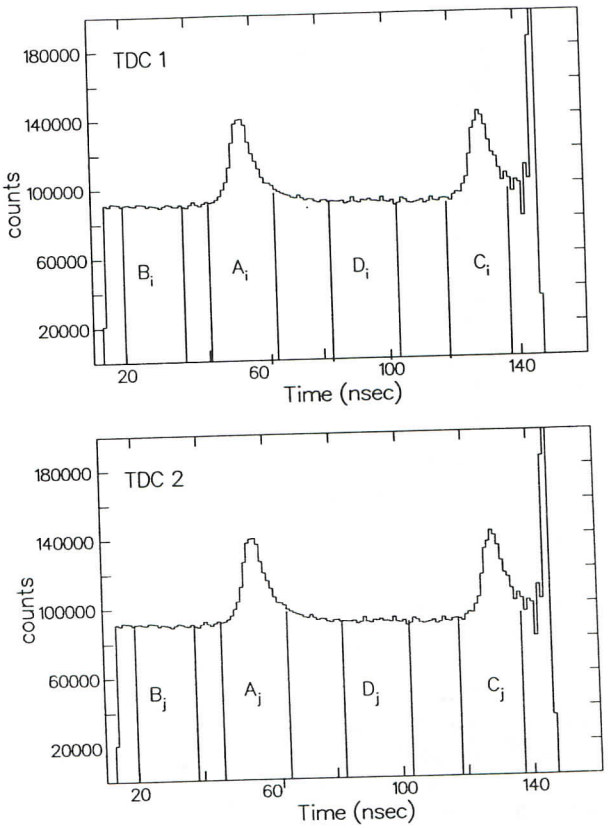

Fig. 7. Singles timing spectra for γ-rays relative to the beam pulse, representing two separate Ge detectors. Using the notation in the text, the figure corresponds to detectors $i = 1$ and $j = 2$ firing. The indicated regions were employed in the technique for extracting true coincidences and achieving background subtraction as described in the text.

Fig. 7. The γ–γ coincidences during the beam pulses are represented by the combinations A_iA_j and C_iC_j where the ith and jth detectors fired for the event. The algorithm

$$(A_iA_j + C_iC_j) - (B_iB_j + D_iD_j) - (A_iC_j + C_iA_j) + (B_iD_j + D_iD_j)$$

performed a suitable subtraction of undesired coincidences. Its effectiveness is illustrated in Fig. 8, in which the total projections of the matrix with and without subtraction are compared.

The coincidence data were sorted into a symmetric $E_{\gamma 1}$ vs. $E_{\gamma 2}$ matrix with background subtraction. Examples of γ–γ coincidence spectra for three of the strongest reaction channels are shown in Fig. 9. These spectra are each the sum of several gates on known transitions in the specified nuclei. Data from all of the germanium detectors have been included, and the gate widths were chosen to allow for Doppler-broadened lineshapes in the case of the 145° detectors. Spectra are shown for the 4p channel (^{55}Fe, [20]), the 3pα channel (^{52}Mn, [22]) and the 3pn channel leading to the mirror nucleus ^{55}Co [19]. The data set from the present work falls short in the number of γ-ray

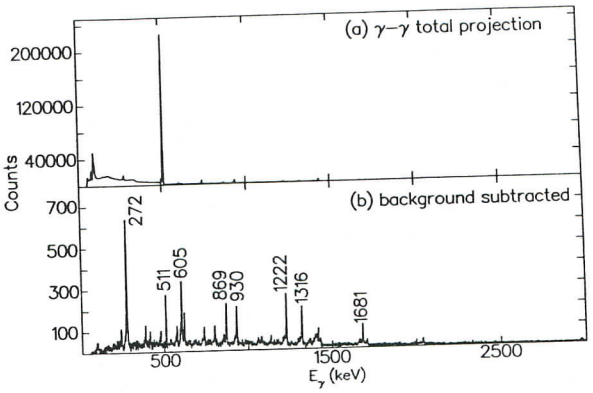

Fig. 8. Total projections of the γ–γ coincidence matrix for the ^{19}Ne beam: (a) without, and (b) with background subtraction.

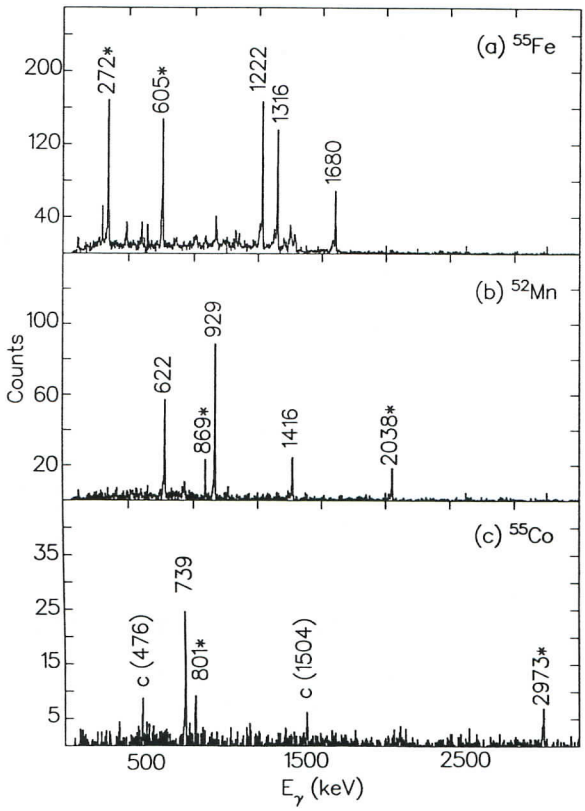

Fig. 9. Random subtracted γ–γ coincidence spectra for (a) sum of gates on 272 keV and 605 keV transitions in ^{55}Fe, (b) sum of gates on 869 keV and 2038 keV transitions in ^{52}Mn, and (c) sum of gates on 801 keV and 2973 keV transitions in ^{55}Co. Gating transitions are labelled with asterisks. Known contaminants in the ^{55}Co spectrum are labelled "c". Data are from all detectors.

coincidences desirable to study new nuclear structure by a factor of approximately 10–100.

3.6. Comparison of radioactive and stable beam results

The timing spectra of Fig. 4 illustrate clearly the major difference between the radioactive beam and the stable beam experiments, namely the intense background due to activity from the beam and target. Leaving this aside, as the preceding analysis shows it to be tractable, the differences between the fully background subtracted spectra for the two beams can be assessed in terms of the potential of radioactive beams for producing neutron-deficient nuclei in fusion-evaporation.

In Fig. 10, the background subtracted γ-ray singles energy spectra from the ^{19}F and ^{19}Ne beam experiments are compared. It is immediately apparent that these spectra are of comparable quality. This is perhaps one of the

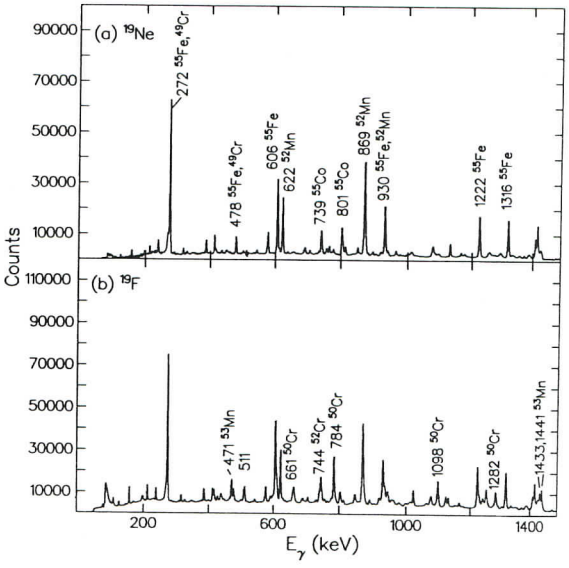

Fig. 10. Comparison of the background subtracted gamma-ray singles spectra for (a) the ^{19}Ne beam, and (b) the ^{19}F beam data. Data from all 90° Ge detectors.

clearest indications that experiments with radioactive beams can be performed successfully.

In the present work, particular interest centred on the $A = 55$ mirror nuclei. No transitions in the yrast decay of ^{55}Ni had been observed previously, and only a few transitions in ^{55}Co [19]. The present data confirm the previous results for ^{55}Co. One transition at 2796 keV, seen only with the ^{19}Ne beam, is a candidate for the mirror in ^{55}Ni of the 2973 keV transition to the ground state in ^{55}Co. The 2796 keV γ-ray was found by analysis of the LEDA data to be associated with strictly less than three charged particles. These results will be described in a separate publication [24].

In Table 3, the relative intensities of γ-rays are displayed for representative transitions in each of the nuclei observed with both beams. A typical strong peak, namely the 1316 keV transition in ^{55}Fe, has been used for normalizing the yields. The ratios $Y(^{19}\mathrm{Ne})/Y(^{19}\mathrm{F})$ as displayed in Table 3 give a measure of the enhancement of particular peaks in the γ-ray energy spectrum when using ^{19}Ne. They indicate a clear enhancement for ^{55}Co and ^{49}Cr in particular, and are summarized in Fig. 11, where the nuclei are listed in order of decreasing enhancement. There is a tendency to favour low values of T_z, the isospin projection. The trends follow those predicted by statistical model calculations using PACE, as shown in Table 3, although there is some discrepancy for the higher T_z nuclei ^{51}Cr and ^{54}Mn. Thus, γ-ray peaks of interest can be enhanced relative to other peaks by using radioactive

Table 3
Relative yields for gamma-ray production, comparing ^{19}Ne and ^{19}F beams and statistical model predictions

Nucleus	[Ref.]	E_γ [keV]	$Y(^{19}\text{Ne})/Y(^{19}\text{F})$[a]	Channel[b] ^{19}Ne/^{19}F	$Y(E_\gamma)/Y(1.316)$[c] ^{19}F	PACE[d] ^{19}Ne [mb]	PACE[d] ^{19}F [mb]
^{55}Co	[19]	2973	2.53±0.31	(3pn)/(2p2n)	0.21±0.03	151	111
		801	1.98±0.17		0.25±0.02		
		739	1.76±0.36		0.25±0.09		
^{53}Mn	[22]	869	1.02±0.06	(3pα)/(2pαn)	1.59±0.14	242	211
		1416	1.18±0.10		0.89±0.09		
		622	1.06±0.10		0.60±0.06		
^{55}Fe	[20]	1316	1.00±0.06	(4p)/(3pn)	1.00±0.09	114	121
		1222	0.93±0.07		1.12±0.20		
		605	0.82±0.07		1.08±0.10		
^{54}Fe	[21]	1409	1.29±0.18	(4pn)/(3p2n)	0.26±0.12	138	98
		411	1.29±0.10		0.13±0.01		
		1130	1.27±0.19		0.19±0.02		
^{56}Co	[25]	276	1.23±0.07	(3p)/(2pn)	0.19±0.02	8	5
^{49}Cr	[23]	812	1.49±0.20	(2p2α)/(p2αn)	0.11±0.02	74	41
^{51}Cr	[26]	1480	0.36±0.11	(4pα)/(3pαn)	0.05±0.01	45	35
^{52}Mn	[27]	704	0.52±0.16	(5p)/(4pm)	0.08±0.01	31	30

[a] Relative yield with ^{19}Ne beam compared to ^{19}F beam, for individual gamma-rays. Normalised arbitrarily to 1.00 for the 1316 keV line in ^{55}Fe (compare Fig. 10).
[b] Evaporation channel from compound nucleus.
[c] Relative intensities of gamma-rays within the spectrum for ^{19}F, corrected for efficiency (but not for feeding) and normalised arbitrarily to 1.00 for the 1316 keV line in ^{55}Fe.
[d] Predicted cross section according to the program PACE [18].

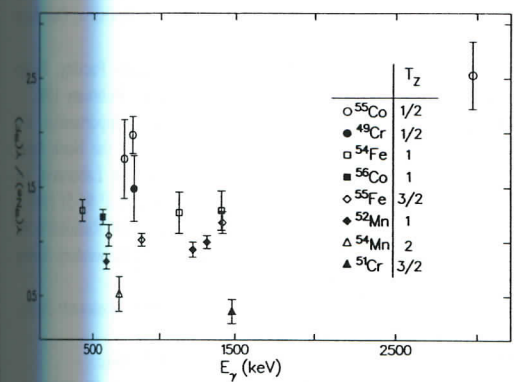

Fig. 11. Relative yields for individual gamma-rays with the radioactive beam ^{19}Ne, compared to the ^{19}F beam. Data are from Table 3. The largest enhancement is for the 2973 keV transition in ^{55}Co. T_z is the isospin projection.

beams to access nuclei far from stability. This factor, together possibly with the opportunity also to select a reaction with an increased cross section, can compensate for reduced intensities of radioactive beams.

4. Conclusions

It has been demonstrated that high spin γ-ray spectroscopy can be performed successfully using an escape suppressed germanium array with an intense radioactive ion beam that produces a large γ-ray background from decay of the beam. Therefore, the choices of reaction for high spin studies can be expanded to take advantage of radioactive beams as they become available. It has proved possible to deal with the particular problems introduced by the β^+ radioactivity of neutron-deficient beam particles and the relatively low beam intensity (as compared with the stable beams). Singles γ-ray and coincidence γ–γ analyses have been shown to produce spectra with very low backgrounds at energies down to 100 keV. Several specific observations may be made about the effectiveness

of Pb-shielding, the beam pulsing and the coincident particle detection, which will be relevant to future experiments.

The need to shield the beam collimators and Compton suppression shields, using approximately 20 mm of Pb, was established during preliminary measurements and implemented in the present work. From inspection of the spectra (e.g. Fig. 10), good Compton suppression was achieved despite the hostile radiation environment. It is apparent that a highly desirable feature of radioactive beams is good quality focussing, comparable with the focussing and stability attained for stable beams with tandem Van de Graaff accelerators.

Charged particle detection proved to be a very useful on-line tool for identifying fusion-evaporation γ-rays. An ideal detector would be compact; in the present work the flight path of ~150 mm introduced a significant time walk into the charged particle detection. The design would also need to address the problems arising from beam particles that elastically scattered from the target and subsequently decayed. The granularity of the silicon detector in the present work and the choice of thickness were each beneficial. The moderate thickness (300 μm) of the silicon allowed protons to be distinguished effectively from α-particles, and this could be improved by reducing the thickness further. Multi-hit probabilities could be deduced for the particles associated with individual γ-ray peaks and, by comparison with binomial probabilities, the number of each type of charged particle could be assigned. This procedure can lead to confident channel identification. The optimum would be a compact pixellated silicon ball close to the target, comprising ~150 μm thick silicon detectors, preferably with further silicon or else scintillators to stop energetic particles. Such a detector would be very useful experimentally in defining the event trigger for the data acquisition.

The beam pulsing was the most important ingredient for producing high quality γ-ray energy spectra. By selecting just those events that occurred during beam pulses, and subtracting a suitable measure of the underlying continuous background, spectacular improvement in the energy spectra was achieved. This was true for both the singles and coincidence γ-ray energy spectra. Thus, experiments using radioactive beams to study γ-ray spectroscopy will best be done using pulsed beams. Experiments to study isomeric states will require an extended or different technique to deal with the background.

The present experiment has provided the first tentative evidence for the ground state transition in the yrast decay of ^{55}Ni. The increases in counting statistics required in order to study new nuclear structure in detail should be achievable with improvements in the detection system. For example, an array of 20 Ge detectors each with a 90% relative efficiency (at 1332 keV) would give two orders of magnitude increase in the γ–γ coincidence efficiency compared to the present work. Thus, high resolution γ-ray spectroscopy is possible with pulsed radioactive beams and germanium γ-ray arrays.

Acknowledgements

S.M. acknowledges support from the Ministry of Culture and Higher Education of Iran. C.S.P. and C.T. acknowledge UK EPSRC student scholarship awards. R.D.P. Is a UK EPSRC Advances Fellow. This work was supported by UK EPSRC research grants, and also performed in the framework of the Belgian Programme on Interuniversity Poles of Attraction initiated by the Belgian State Federal Services of Scientific, Technical and Cultural Affairs.

References

[1] J.O. Newton, in: Nuclear Spectroscopy and Reactions, Part C, ed. J. Cerny (Academic Press, New York, 1974) p. 185.
[2] D. Pelte and D. Schwalm, in: Heavy Ion Collisions, Vol. 3, ed. R. Bock (North Holland, Amsterdam, 1982) p. 1.
[3] European Radioactive Beam Facilities, published by the Nuclear Physics European Collaboration Committee (NuPECC), May 1993, c/o Physikdepartment E12 der T.U. München, D-85748 Germany.
[4] The SPIRAL Radioactive Ion Beam Facility, GANIL R94-02, May 1994.
[5] J.R.J. Bennett, T.A. Broom, C.J. Densham, I.S.K. Gardner, T. Aitken, H.G. Price, D.D. Warner, W. Gelletly and R. Chapman, Proc. Workshop on the Production and Use of Intense Radioactive Beams at the IsoSpin Laboratory, Oak Ridge National Laboratory, Tennessee, 1992, ORNL preprint CONF-9210121, p. 289.
[6] Proc. ISAC workshop, Lake Louise, Canada, Feb 1994, TRIUMF report TRI-94-1.
[7] A Proposal for Physics with Exotic Beams at the Holifield Heavy-Ion Research Facility, Physics Division, Oak Ridge National Laboratory, February 1991.
[8] Concept for an advanced Exotic Beam Facility, Physics Division, Argonne National Laboratory, February 1995.
[9] The IsoSpin Laboratory, Research Opportunities with Radioactive Nuclear Beams, prepared by the North American Steering Committee for the IsoSpin Laboratory, Los Alamos National Laboratory preprint LALP 91-51 (1991).
[10] Overview of Research Opportunities with Radioactive Nuclear Beams, published by the IsoSpin Laboratory Steering Committee, February 1995.
[11] RI Beam Factory, RIKEN accelerator Research Facility, August 1994.
[12] T. Nomura, Nucl. Phys. A 557 (1993) 691c.
[13] P. Darquennes, P. Decrock, Th. Delbar, W. Galster, M. Huyse, Y. Jongen, M. Lacroix, P. Leleux, I. Licot, E. Liénard, P. Lipnik, M. Loiselet, G. Ryckewaert, Sindano Wa Kitwanga, P. Van Duppen, J. Vanhorenbeeck, J. Vervier and S. Zaremba, Phys. Rev. C 42 (1990) R804.

[14] M. Loiselet, N. Postiau, G. Ryckewaert, R. Coszach, Th. Delbar, W. Galster, P. Leleux, I. Licot, E. Liénard, P. Lipnik, C. Michotte, J. Vervier, P. Decrock, M. Gaelens, M. Huyse, G. Vancraeynest, P. Van Duppen, F. Binon, P. Duhamel and J. Vanhorenbeeck, Proc. 3rd Int. Conf. on Radioactive Nuclear Beams, Michigan State University, East Lansing, Michigan, USA, May 1993, ed. D.J. Morrissey (Editions Frontières, Gif-sur-Yvette, 1993) p. 179.

[15] P.J. Nolan, D.W. Gifford and P.J. Twin, Nucl. Instr. and Meth. A 236 (1985) 95.

[16] T. Davinson, A.C. Shotter, E.W. MacDonald, S.V. Springham, P. Jobanputra, A.J. Stephens and S.L. Thomas, Nucl. Instr. and Meth. A 288 (1990) 245.

[17] S.L. Thomas, T. Davinson and A.C. Shotter, Nucl. Instr. and Meth. A 288 (1990) 212.

[18] A. Gavron, in: Computational Nuclear Physics 2, eds. K. Langanke, J.A. Maruhn and S.E. Koonin (Springer, New York, 1993) p. 108.

[19] M.G. Saint-Laurent, Sl. Cavallaro, M.L. Sperduto, B. Delaunay, J. Delaunay and H. Dumont, Z. Phys. A 334 (1989) 365.

[20] H. Fromm, H.V. Klapdor and P. Herges, J. Phys. (London) G 7 (1981) L109.

[21] E. Dafni, J.W. Noé, M.H. Rafailovich and G.D. Sprouse, Phys. Lett. B 76 (1978) 51.

[22] L.R. Medsker, L.H. Fry, Jr. and D.C. Wilson, Phys. Rev. C 18 (1978) 2584.

[23] J.A. Cameron, M.A. Bentley, A.M. Bruce, R.A. Cunningham, W. Gelletly, H.G. Price, J. Simpson, D.D. Warner and A.N. James, Phys. Lett. B 235 (1990) 239.

[24] S. Mohammadi et al., to be published.

[25] N. Bendjaballah, J. Delaunay and H.J. Kim, Nucl. Phys. A 244 (1975) 322.

[26] A. Dauchy, A. Giorni, D.H. Koang, J.P. Longequene, B. Chambon, D. Drain and C. Pastor, Phys. Lett. B 82 (1976) 365.

[27] M. Toulemonde, F.A. Beck, C. Gehringer, B. Haas, J.C. Merdinger, N. Schultz and J.P. Vivien, J. Phys. (London) G 5 (1979) 819.